Autonomic Self-Healing of PEDOT:PSS Achieved Via Polyethylene Glycol Addition

*Yang Li, Xinda Li, Shiming Zhang, Leslie Liu, Natalie Hamad, Sanyasi Rao Bobbara, Damiano Pasini, and Fabio Cicoira**

Self-healing electronic materials are of primary interest for bioelectronics and sustainable electronics. In this work, autonomic self-healing of films obtained from mixtures of the conducting polymer poly(3,4-ethylenedioxythiophene) doped with polystyrene sulfonate (PEDOT:PSS) and polyethylene glycol (PEG) is reported. The presence of PEG in PEDOT:PSS films decreases the elastic modulus and increases the elongation at break, thus leading to a softer material with enhanced self-healing characteristics. In situ imaging of the cutting/healing process shows that the healing mechanism is likely due to flowing back of the material to the damaged area right after the cutting.

1. Introduction

Self-healing materials are able to recover their functionalities after being damaged, via a process that can be spontaneous (autonomic), or triggered by an external input.[1–8] Materials showing autonomic self-healing are highly desired, in particular for applications such as bioelectronics and wearable electronics, where frequent damages may occur due to mechanical movement or prolonged contact with living tissues and biological fluids.[9–17] Several approaches have been proposed to achieve such kind of materials. Song et al. reported an aerogel framework fabricated via in situ polymerization of *N*-isopropylacrylamide on sulfur-containing Ag nanowires with an electrical conductivity of 93 S cm^{-1}, exhibiting autonomic self-healing due to the strong reversible Ag—S bonds.[18] Autonomic self-healing, resulting from ion-dipole interactions, was also found in ionic conductors consisting of ionic liquids in a poly(vinylidene fluoride-*co*-hexafluoropropylene) matrix, which showed a conductivity ranging between ≈10^{-5} and 10^{-9} S cm^{-1}.[5,19] Lu et al. reported autonomic self-healing of a stretchable polymer complex composed of poly(2-acrylamido-2-methyl-1-propanesulfonic acid), poly-aniline and phytic acid, which also acts as a strain sensor.[20] Other types of autonomic self-healing materials make use of micro-capsules of conductive agents, such as liquid metal or silver paste, embedded into a polymer matrix.[21–35]

The conducting polymer poly(3,4-ethylenedioxythiophene) doped with polystyrenesulfonic acid (PEDOT:PSS) is attracting enormous interest as self-healing material, due to its widespread use in bioelectronics and wearable electronics. Our group demonstrated that PEDOT:PSS films can be healed electrically by water after being cut by a razor blade and show autonomic self-healing when wetted with water before being cut.[36] However, wet PEDOT:PSS films are extremely fragile and their autonomic healing behavior vanishes after drying. A possible strategy to achieve autonomic self-healing in PEDOT:PSS films is to modify their mechanical properties via mixing with other polymers. Along this line, it has been shown that mixtures of PEDOT:PSS with the surfactant Triton X-100 show autonomic self-healing and can be used for deformable electronics and stretchable thermoelectrics.[6,8] However, as Triton X-100 is potentially harmful,[37] alternative approaches need to be explored to develop self-healing materials for applications in bioelectronics.

We have recently reported that adding polyethylene glycol (PEG) to PEDOT:PSS films significantly improves the performance of stretchable organic electrochemical transistors, by reducing the density of the cracks in the films upon stretching.[38] PEG, also known to act as a moderate electrical conductivity enhancer for PEDOT:PSS,[38–40] has been already used to modify the mechanical properties of several polymers, by decreasing the Young's modulus and increasing the elongation at break.[41,42] The biocompatibility and anti-fouling properties of PEG make it interesting for applications in bioelectronics.[43–45] On the basis of these results, we believe that the presence of PEG in PEDOT:PSS films can lead to significant changes of the self-healing properties. In this work we explore the self-healing properties of films obtained from blends of PEDOT:PSS and PEG. We show that films processed from a mixture of PEDOT:PSS aqueous suspension and PEG exhibit repeatable autonomic self-healing when cut by sharp blades,

Y. Li, Dr. X. Li, L. Liu, N. Hamad, Dr. S. R. Bobbara, Prof. F. Cicoira
Department of Chemical Engineering
Polytechnique Montréal
Montréal, QC H3C3J7, Canada
E-mail: fabio.cicoira@polymtl.ca
Dr. S. Zhang
Center for Minimally Invasive Therapeutics
California NanoSystems Institute
University of California
Los Angeles, CA 90095, USA
Prof. D. Pasini
Department of Mechanical Engineering
McGill University
Montreal, QC H3A0C3, Canada

even in presence of the conductivity enhancer glycerol. The self-healing can be switched from autonomic to water-enabled by varying the PEG amount in the film, the molecular weight of PEG or by soaking PEG-containing films in methanol. We found that the addition of PEG decreases the Young's modulus and increases the elongation at break of PEDOT:PSS films, thus leading to a soft and viscoelastic material.

2. Results and Discussion

Preliminary experiments revealed that to achieve films showing autonomic healing, at least 3% PEG needs to be added to the PEDOT:PSS aqueous suspension. The addition of lower amounts leads to water induced healing. For our studies we focused on films obtained from mixtures of PEDOT:PSS and 4% PEG-400, as this composition is safely beyond the threshold required for autonomic self-healing. Free standing films obtained from mixtures of PEDOT:PSS and 4% PEG-400 (thickness ≈15 µm, electrical conductivity ≈200 S cm^{-1}) show autonomic self-healing upon multiple cuts (black curve in **Figure 1**a, Figure S1, Video S1, Supporting Information), with a healing efficiency close to 100%. An identical behavior was observed when 5 v/v% glycerol was added to the processing mixture, leading to an increase of the electrical conductivity to ≈400 S cm^{-1} (cyan curve in Figure 1a). The time-lapse current measurements (Figure 1b) show that the process takes place rapidly, with healing times ranging between ≈50 and 800 ms. The autonomic self-healing is observed for cut widths ranging between ≈10 and 60 µm (i.e., about 4 times the film

thickness), achieved with blades of different sharpness (Table S1, Supporting Information). The SEM images of healed films (Figure 1c,d, Figure S3, Supporting Information) show that, although the damage induced by the blade can be clearly distinguished, there are no discontinuities between the two sides of the cut. The autonomic self-healing vanishes when the cut width is increased to ≈100 µm, using the edge of a quartz microscope slide (Figure S2, Supporting Information).

As shown above, the addition of PEG to the films processing mixture is essential to achieve autonomic self-healing. To confirm that PEG is still present at the end of the film processing, we performed thermogravimetric analysis (TGA, **Figure 2**a) and Fourier-transform infrared spectroscopy (FTIR, Figure S4, Supporting Information). TGA curves of pristine PEDOT:PSS films show a sharp weight loss above 300 °C, due to the decomposition of thiophene.[46] Films containing PEG-400 show a different behavior, with a main weight loss occurring between 150 and 300 °C, likely due to the vaporization of PEG-400. The weight loss is more pronounced for samples containing 4 v/v% and 10 v/v% PEG-400, where it reaches ≈80%. In the FTIR spectra, the peaks at 2875 cm^{-1} (C−H stretching) and 1645 cm^{-1} (C−O−H bending), as well as the broad band at 3300 cm^{-1} (O−H stretching band of the hydroxyl group), confirm the presence of PEG in the films.[39,47–49] The intensities of the peaks at 2875 and 1645 cm^{-1} and of the broad band gradually increase with increasing PEG amount (Figure S4, Supporting Information), which indicates that the hydroxyl groups of PEG form hydrogen bonding with the hydroxyl groups of other PEG molecules and with the sulfonate groups of PEDOT:PSS.[47–49] The total hydrogen bonding contribution is enhanced with the increase
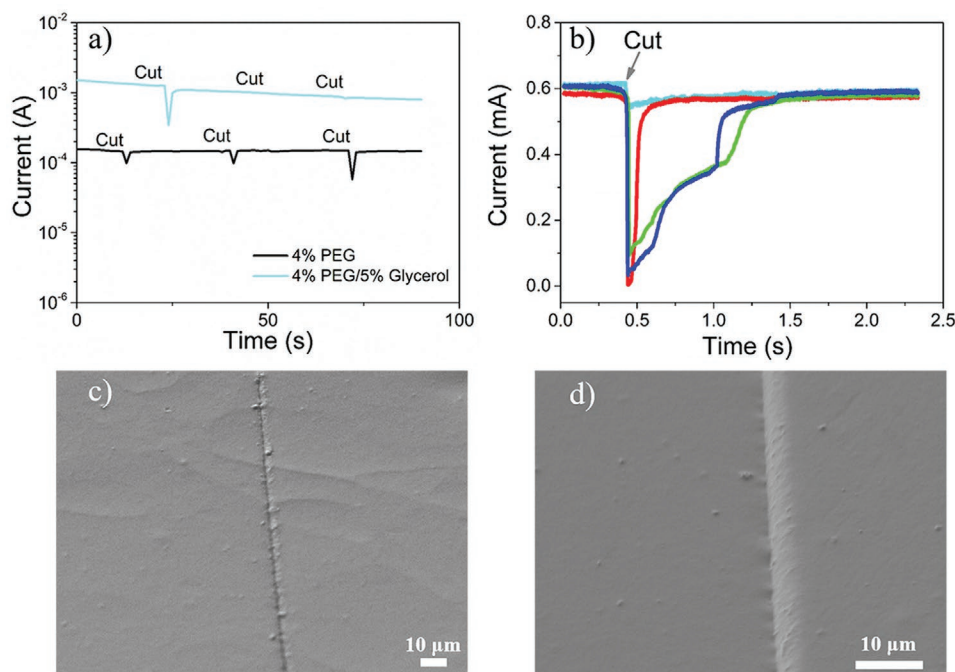

Figure 1. a) Current versus time plots during several cuts in different regions of films processed from mixtures containing PEDOT:PSS and 4% PEG-400, with or without 5% glycerol. b) Time-lapse current measurements during the cut/healing process for four different films processed from mixtures containing PEDOT:PSS and 4% PEG-400. c,d) SEM images of the cut and healed region with different magnifications. The voltage applied during the healing test was 0.2 V. The thickness of the films was ≈15 µm.
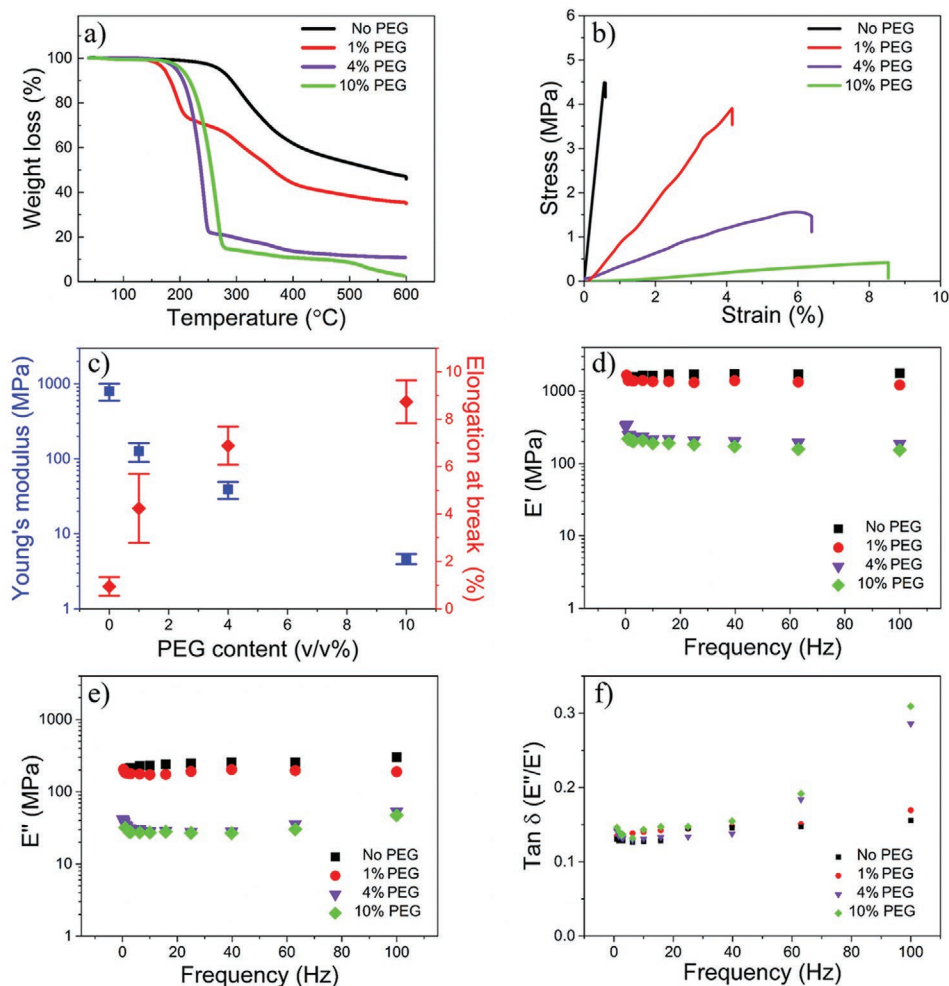
Figure 2. Thermal and mechanical properties of films processed from mixtures of PEDOT:PSS and different amounts of PEG-400. a) Thermogravimetric analysis; b) stress–strain curves; c) Young's modulus and break elongation as a function of the PEG-400 content; d) storage modulus (E′); e) loss modulus (E″); f) mechanical damping factor (tan δ = E″/E′) for different PEG-400 contents, obtained via DMA in the frequency range 100–0.01 Hz. The thickness of the films used for mechanical tests was ≈100–150 μm.

of PEG amount, due to the availability of more hydroxyl groups. This is also reflected in the shift of onset temperature for weight decrease in the TGA curves of conducting polymer films containing larger amounts of PEG-400 (Figure 2a).[49–51] The presence of PEG is further confirmed by X-ray photoelectron spectroscopy (XPS), via the shift of C(1s) and O(1s) core level spectra (Figure S5, Supporting Information), in agreement with our recent work.[38]

To evaluate the impact of PEG on the mechanical properties of the films under study, we performed tensile stress–strain measurements and dynamic mechanical analysis (DMA) of PEDOT:PSS films processed from pristine PEDOT:PSS solution and from PEDOT:PSS solutions containing different concentrations of PEG-400. A maximum of 10% PEG was added to the PEDOT:PSS processing solution, as higher amounts (≈15%) yielded a dough-like suspension, which could not be used to make freestanding films. Stress-strain responses (Figure 2b and Figure S6, Supporting Information) show almost linear behavior for all films. Additionally, as the PEG content increases the slope (Young's modulus) decreases. Pristine PEDOT:PSS

films show elongation at break (percentage increase in length that occurs before breaking under tension) of ≈0.5% upon application of a stress of ≈4.5 MPa. Increasing the PEG content leads to an increase of the elongation at break, that is, ≈4% upon application of a stress of ≈3.8 MPa for 1 v/v% PEG-400, ≈6.5% upon application of a stress of ≈1.5 MPa for 4 v/v% PEG-400 and ≈8.5% upon application of a stress of ≈0.3 MPa for 10 v/v% PEG-400. The plots of the Young's modulus and the elongation at break (versus the amount of PEG in the film processing mixture (Figure 2c, data extracted from the stress–strain responses shown in Figure S6, Supporting Information) show that increasing the PEG content leads to a gradual decrease of the modulus from ≈800 MPa (pristine PEDOT:PSS) to ≈4 MPa (10 v/v% PEG), and a gradual increase of the elongation at break from ≈1% to ≈9%. These results clearly indicate that increasing the amount of PEG leads to softer films. It is important to point out that the film conductivity increases from a few S cm⁻¹ to ≈350 S cm⁻¹ upon addition of 1% PEG, then decreases to ≈200 S cm⁻¹ upon addition of 4% PEG (**Table 1**). To investigate the viscoelastic properties, we performed DMA

Table 1. Summary of healing behaviors and electrical conductivity of PEDOT:PSS/PEG films.

Processing mixture/treatment	Healing behavior	Electrical conductivity [S cm^{-1}]
PEDOT:PSS/1%PEG-400	Water-enabled	356 ± 23
PEDOT:PSS/4%PEG-400	Autonomic	201 ± 13
PEDOT:PSS/4%PEG-400/5%Glycerol	Autonomic	373 ± 52
PEDOT:PSS/4%PEG-400 after methanol soaking	Water-enabled	1399 ± 87
PEDOT:PSS/4%PEG-200	Autonomic	237 ± 27
PEDOT:PSS/4%PEG-1500	Autonomic	118 ± 15
PEDOT:PSS/4%PEO-100000	Partial autonomic and water-enabled	58 ± 13
PEDOT:PSS/4%PEO-5000000	Water-enabled	17 ± 9

at variable stress frequencies. The storage modulus E′, which is a measure of the elastic response, does not show a strong dependence on frequency, whereas the loss modulus E″, which expresses the viscous response, increases with frequency. Both E′ and E″ decrease with increased PEG content, especially at concentrations of 4 and 10 v/v% PEG (Figure 2d,e), with the viscous component remaining lower than the elastic one. The behavior of E′ parallels that of the Young's modulus and confirms that the addition of PEG leads to softer films. The relative ratio (tan δ = E″/E′) between loss and storage modulus (damping factor) is almost constant for all films up to a frequency of 40 Hz. In the 40–100 Hz range it shows a steep increase for 4 and 10 v/v% PEG contents (Figure 2f). The latter result points to an increased tendency of the material to dissipate energy, that is, to a more pronounced viscoelastic behavior, likely due to the mobility of the PEG chains.

Although further investigations are needed to establish a clear correlation between mechanical properties and self-healing behavior, our results suggest that autonomic self-healing is favored by the softness and viscoelasticity provided to PEDOT:PSS films by increasing amounts of PEG. For instance, films processed from mixtures containing 4% PEG, characterized by a pronounced softness and viscoelasticity, show autonomic self-healing. On the other hand, decreasing the amount of PEG to 1%, leads to mechanical properties similar to those of pristine PEDOT:PSS and, as a consequence, to a change from autonomic to water-induced healing (**Figure 3**a,b).[36] SEM images confirm that the gap of ≈15 μm created by the cut (Figure 3c) is fully healed by water (Figure 3d).

With the aim to increase the conductivity of autonomically healable films, we carried out methanol soaking (20 min followed by 20 min drying at 140 °C),[52–54] which led to an increase from ≈200 S cm^{-1} to ≈1400 S cm^{-1} (Table 1). TGA curves (Figure 3e) show that this treatment leads to a behavior similar to pristine PEDOT:PSS films, thus indicating that the conductivity enhancement is most likely due to the dissolution of the insulating PEG during methanol soaking.[52–54] The PEG dissolution, however, led to a switch from autonomic to water-enabled healing (Figure 3f). Re-immersing the films in PEG for about 30 min led only to a partial recovery of the autonomic healing (Figure S7, Supporting Information). Therefore,

although it suppresses autonomic healing, methanol soaking can be exploited to achieve water-healable films with high conductivity. The self-healing performance of PEG containing PEDOT:PSS films also depends on the molecular weight of PEG. In addition to PEG-400, we investigated PEG-200, PEG-1500, PEO-100000, and PEO-5000000, by keeping the added amount constant to 4 v/v%. Films containing PEG-200 show autonomic healing (Figure S8a, Supporting Information) and a conductivity similar to that achieved with PEG-400. The use of PEG-1500 leads to a decrease of the healing efficiency to ≈80% (Figure S8b, Supporting Information). Films containing polyethylene oxide (PEO, molecular weight 100 000) show a partial autonomic healing, which can be completed by wetting the damaged area with water (Figure S8c, Supporting Information). Films containing PEO-5000000 show only water-enabled healing (Figure S8d, Supporting Information). This decrease in autonomic healing efficiency can be attributed to the lower mobility of the longer chains of high molecular weight PEG, which may lead to increased stiffness, thus hindering the flow back of material to the damaged area after cut. It is also worth noticing that increasing the molecular weight of PEG results in a significant conductivity decrease, as reported in the literature.[39] The self-healing behavior and the electrical conductivity of films processed from different PEDOT:PSS/PEG mixtures are summarized in Table 1.

In our previous work, we hypothesized that swelling may play a role in the mechanism of water induced healing.[36] To validate our hypothesis, here we measured the swelling (i.e., weight gain upon water immersion) of PEDOT:PSS films containing various amount of PEG-400 (**Figure 4**a). As pristine PEDOT:PSS films were too brittle to handle for this experiment, we replaced them with films containing 5% of glycerol. Soaking for 10 min in water led to a weight increase of ≈300% for PEDOT:PSS films containing glycerol and 1% PEG. This high swelling ability may explain the water-enabled self-healing. A higher amount of PEG causes the weight increase to drop to ≈90% for 2 v/v% PEG-400 and ≈30% for 4 v/v% PEG-400. No further changes were observed upon soaking for longer times. Interestingly, upon increasing the PEG content, the weight of dry films increases, in accordance with TGA (Figure 2a), while that of wet films remains almost constant (Figure 4b). A similar trend was observed by exposing the films to water vapor in a humidity chamber with a relative humidity (RH) of ≈95% (Figure S9, Supporting Information). In agreement with the literature, the reduced swelling of films containing PEG is likely due to partial removal of PSS, which is responsible of the high swelling of PEDOT:PSS.[55–57] A similar behavior is found for the surfactant Triton X-100, which has also been reported to induce autonomic healing of PEDOT:PSS films (Figure S10, Supporting Information).[6,8] We found that Triton-containing PEDOT:PSS films show autonomic or water-enabled healing depending on the amount added to PEDOT:PSS (Figure S11, Supporting Information), as in the case of PEG.

To prove that swelling does not play a significant role in autonomic healing of PEDOT:PSS films containing 4% PEG, we performed cut/healing experiments in dry conditions in a N$_2$ purged glove box, after baking the film in situ for 14 h at 140 °C. Notably, the autonomic self-healing after multiple cuts was observed even in these conditions (Figure S12, Supporting
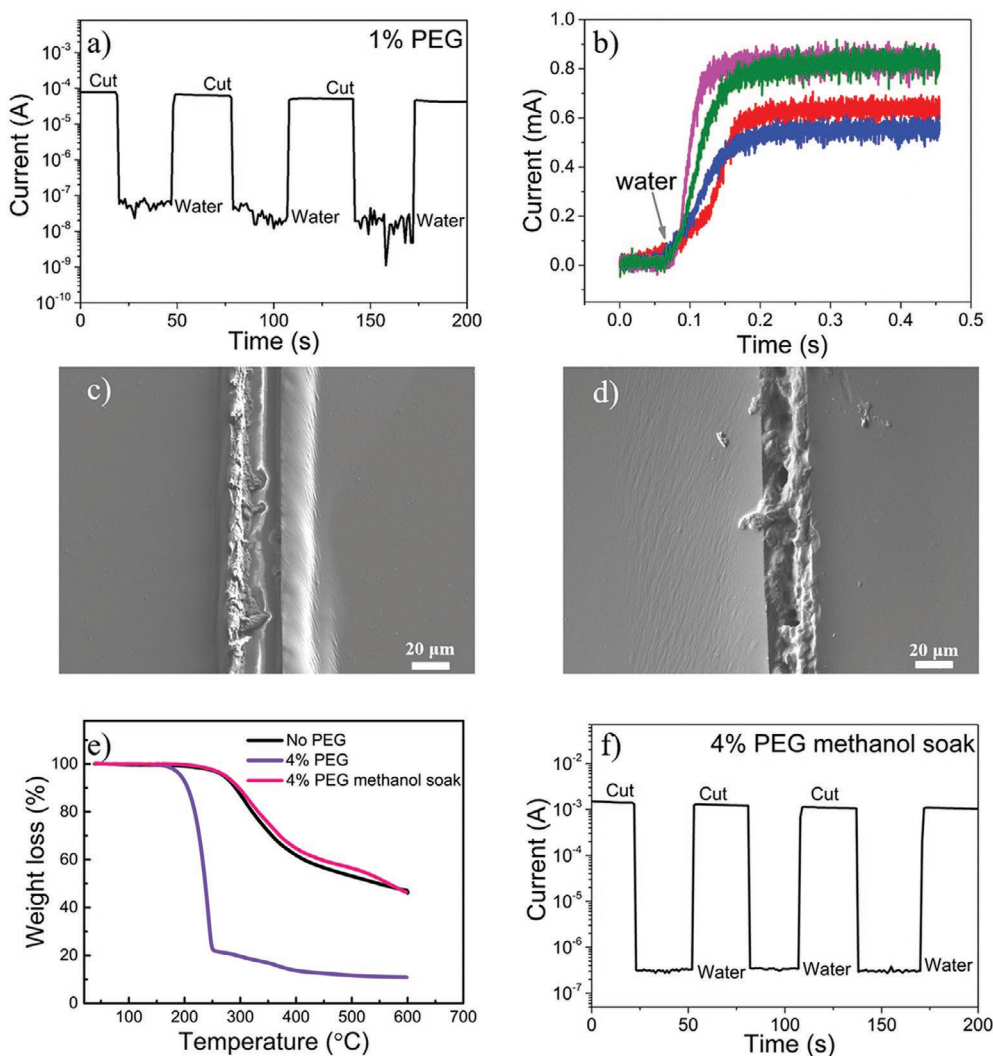
**ADVANCED
SCIENCE NEWS**

www.advancedsciencenews.com

**ADVANCED
FUNCTIONAL
MATERIALS**

www.afm-journal.de

Figure 3. a) Current versus time plot of a film processed from a mixture containing PEDOT:PSS and 1% PEG-400 during several cuts and water healings in different regions; b) time-lapse current measurements of the healing process of PEDOT:PSS/1%PEG films; SEM images of the damaged area c) before and d) after healing; e) TGA curves of PEG containing PEDOT:PSS films before and after soaking in methanol compared to pristine PEDOT:PSS films; f) current versus time plot of a film processed from a mixture containing PEDOT:PSS and 4% PEG-400 and rinsed in methanol upon several cuts and water healings in different regions. The voltage applied during the healing test was 0.2 V. The thickness of the films was ≈15 μm (methanol soaking can lead to a thickness decrease).
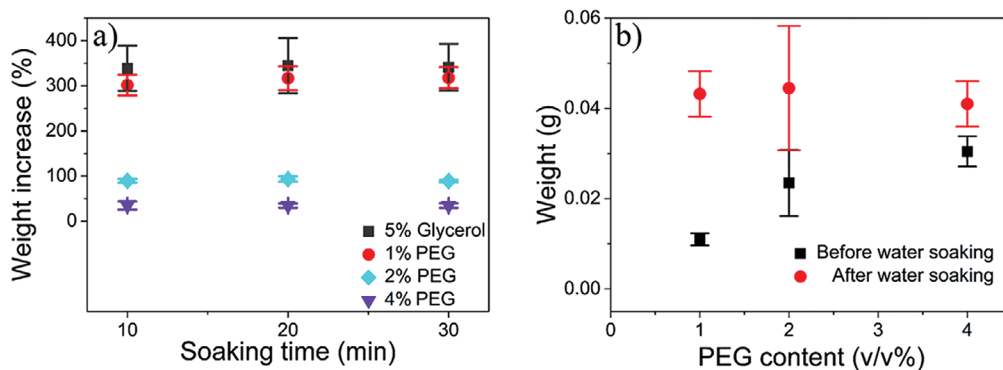

Figure 4. a) Weight increase versus water soaking time of PEDOT:PSS films containing different amounts of PEG-400; b) weight of PEDOT:PSS films containing different amounts of PEG-400 before and after water soaking for 10 min.

**ADVANCED
SCIENCE NEWS**

www.advancedsciencenews.com

**ADVANCED
FUNCTIONAL
MATERIALS**

www.afm-journal.de

Information), thus excluding any significant role of water trapped in the hygroscopic PEG matrix. The limited swelling provides PEG-containing PEDOT:PSS films with an excellent stability during wetting and drying cycles, while pristine PEDOT:PSS films show a considerable shrinking in the same conditions (Figure S13, Supporting Information). This property can be exploited for the fabrication of electrodes for biomedical devices operated under high humidity conditions, e.g. in incubators for neonatal intensive care units, where swelling can cause dramatic shape change, leading to detachment from the skin and device failure.

To further investigate the healing process, we performed in situ imaging of the cut/healing process, using a micro scratcher equipped with an inverted optical microscope. Imaging during the cutting process (Video S2, Supporting Information, and **Figure 5**a, where the brighter part corresponds to the blade and the dark part to the film being cut) reveals that the gap created by the cut becomes narrower as

the blade moves forward. Imaging right after completion of the cut shows that the gap is completely healed and no longer visible (Video S3, Supporting Information, Figure 5b), in agreement with SEM images. These results clearly indicate that, just after being cut, the material rapidly flows back to the damaged area, likely due to the viscoelastic properties imparted by PEG.

It has been reported that PEG chains present in the films screen the ionic interaction between PEDOT and PSS by forming hydrogen bonding with PSS. This leads to a phase separation between PEDOT and PSS, and favors the formation of aggregated PEDOT domains, enhancing the film conductivity (Scheme I in Figure 5c).[39] The PEG chains also function as a soft matrix for PEDOT:PSS particles and endow a well-mixed and strong entanglement between hydrophilic PSS chains, thus favoring the flowing-back of material towards the damaged area after cutting (Scheme II in Figure 5c). A further contribution to the healing process, and thus to the rebuilding of the
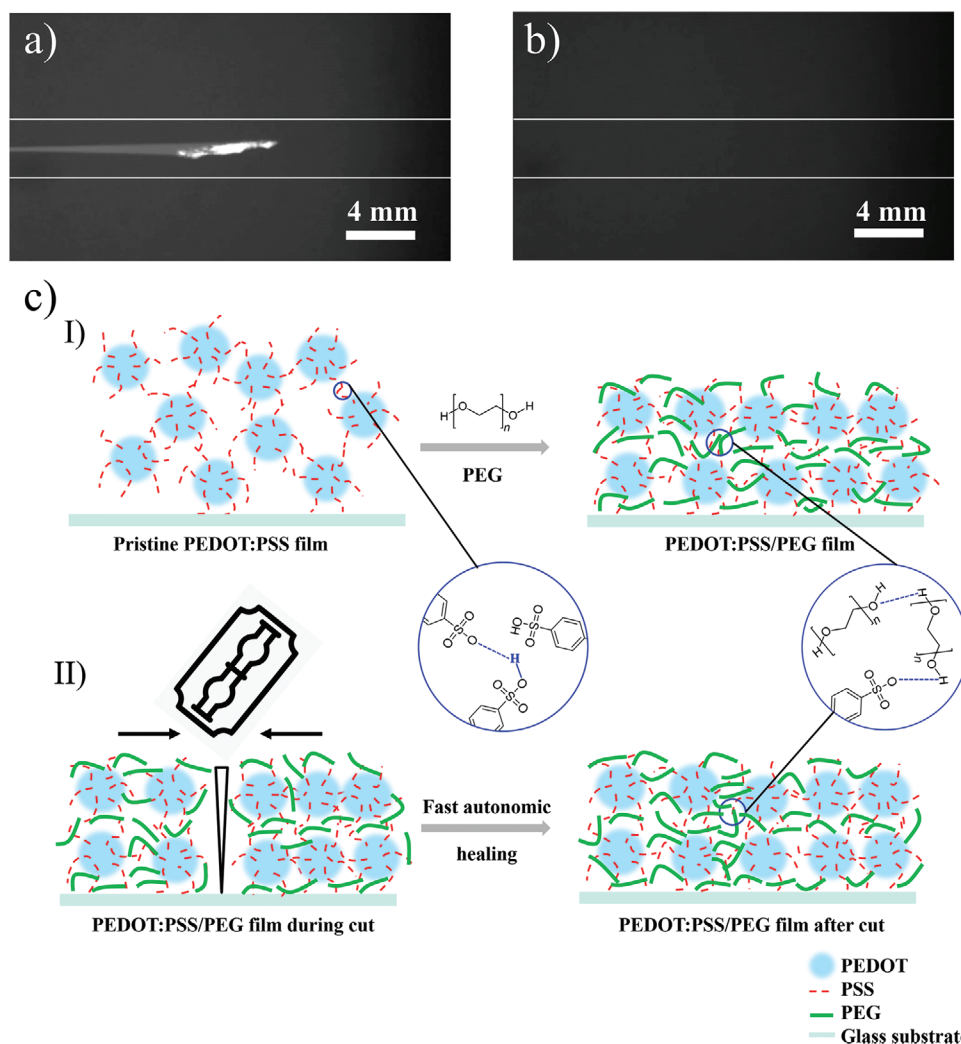

Figure 5. a) Optical images of a PEDOT:PSS/PEG film while being cut by the micro scratcher and b) after the cut. The white lines have been added to highlight the cut region. c,I) Scheme of the soft matrix effect played by PEG chains in PEDOT:PSS films; c,II) Scheme of the proposed mechanism for the autonomic healing of PEDOT:PSS/PEG film. The chemical structures in the circles represent the H-bonds between two PSS chains, between two PEG chains, and between a PSS and a PEG chain.

ADVANCED
SCIENCE NEWS
www.advancedsciencenews.com

ADVANCED
FUNCTIONAL
MATERIALS
www.afm-journal.de

PEDOT-PEDOT conducting pathways in the PEG matrix, might be the formation of hydrogen bonds between PEG-PEG, PSS-PSS, and PEG-PSS chains at the interfaces of the gap (Scheme II in Figure 2c).[6,8,39,58]

3. Conclusion

We have shown that PEDOT:PSS films containing PEG-400 show autonomic self-healing in dry conditions, even in the presence of the conductivity enhancer glycerol. In situ imaging of the cutting/healing process shows that, just after cutting, the two parts of the film reconnect by flowing back to the damaged area. The autonomic self-healing is attributed to the change of mechanical properties induced by PEG, which leads to a lower elastic modulus, a larger elongation at break and more enhanced viscoelastic properties with respect to pristine PEDOT:PSS films. The self-healing behavior of PEDOT:PSS/PEG films depends on the molecular weight and the amount of the PEG added to the processing mixture. Low-molecular weight PEG (200 and 400) favors autonomic self-healing, likely because of the high mobility of short molecular chains. Films containing higher molecular weight PEG (1500 or 10 000) or a lower amount of PEG (e.g., 1 v/v %) do not heal autonomically and rather show water induced healing, which can be explained by water swelling of the films. We believe that this work will propel the development of healable electronics for wearable or biomedical applications.

4. Experimental Section

Materials: The PEDOT:PSS aqueous suspension (Clevios PH1000) was purchased from Heraeus Electronic Materials GmbH (Leverkusen, Germany). Glycerol (99.5+% purity) was purchased from Caledon Laboratories Ltd. (Georgetown, ON). PEG 200, 400, and 1500, PEO 1 00 000 and 50 00 000 and the liquid metal gallium–indium eutectic (EGaIn 495 425) were purchased from Millipore Sigma. All chemicals were used without further treatment. Glass slides (Corning 2947–75 × 50) were purchased from Corning Incorporated.

Processing and Characterization of PEDOT:PSS Films: The mixtures to process the films were prepared by mixing Clevios PH1000 with PEG or PEO and glycerol in a centrifugal mixer (Thinky M310) at 2000 rpm for 5 min. As PEG-1500, 1 00 000, and 50 00 000 are solid at room temperature, their volume was calculated by dividing the weight by the density. The films were deposited by drop-casting (≈0.5 mL of mixture) on glass slides and successively baked on a hot plate with the following sequence: 50 °C for 1 h, 90 °C for 2 h, and finally 140 °C for 6 h. The gradual temperature increase permitted to obtain continuous films without the formation of bubbles, which could be easily detached from the glass slides.[36] The film thickness was measured with a profilometer (Dektak 150) using a 12.5 μm stylus tip with a 10 mg load. Optical microscopy images were obtained with a Carl Zeiss Axio microscope. SEM measurements were performed with a JEOL JSM-7600TFE field emission scanning electron microscope with a voltage of 5.0 kV (LEI) under a vacuum of 10⁻⁴ Pa. XPS was performed using a VG ESCALAB 3MKII system with Mg-Ka X-ray source in an ultra-high vacuum. FTIR was performed using a PerkinElmer FTIR Spectrum Two spectrometer. Electrical conductivity measurements were carried out on thin films (thickness ≈200 nm) deposited by spin-coating at 1000 rpm and baked at 140 °C for 1 h. Sheet resistances were measured by a four-point probe (Jandel engineering) connected to an Agilent B2902A voltage-current source measure unit.

Self-Healing Tests: Self-healing experiments were carried out in ambient air on films with a size of ≈(6.0 × 1.5) cm, and a thickness of ≈15 μm. Electrical contacts were made via two tungsten probes immersed into EGaIn contacts at the two sides of the film and the current was measured with an electrical probe station equipped with national instruments NI PXIe-1062Q source-measure unit controlled by Labview software. The cuts for the self-healing experiments were performed manually using different razor, surgical and ceramic blades (specifications reported in Table S1, Supporting Information) and a quartz microscope slide (Micro-Tec 51–001113, (76.2 × 25.4 mm) × 1 mm). The size of the cuts induced by the different blades was measured on pristine PEDOT:PSS films, which do not show autonomic healing. A droplet (≈40 μL) of deionized (DI) water (18.2 MΩ cm at 25 °C, Millipore) was used as the healing agent for water-enabled healing experiments. The time for current recovery is referred as the healing time; the ratio $\eta = \frac{I_{healed} - I_{damaged}}{I_{pristine} - I_{damaged}}$, where I is the current measured for pristine, damaged, and healed films, as the healing efficiency. For the time-lapse current measurement, the PEDOT:PSS/PEG film was connected with a sensing series resistor. The output voltage on the sensing resistor was measured after applying 100 mV of input voltage. The plotted current was calculated from the relation $I = V_{resistor}/R$. The actual voltage drop across the PEDOT:PSS/PEG films under test was less than 100 mV. For real time imaging of the cutting/healing processes, the cuts were performed with titanium-coated trimmer blades (Fiskars) mounted a Micro Scratcher (MST³, CSM instruments SA) equipped with an inverted microscope (Zeiss Axioscope A1). The force applied by the cutting blade to the film was 200 mN and the blade moving speed was 2 cm min⁻¹.

Thermogravimetric Analysis: TGA was performed on a TG Q500 (TA Instruments). 5 mg samples of pristine PEDOT:PSS film or PEDOT:PSS/PEG films were transferred into platinum pans to perform the test. The TGA curves were acquired between 40 and 600 °C (heating rate of 10 °C s⁻¹) under nitrogen atmosphere (flow rate of 60 mL min⁻¹).

Mechanical Tests: Tensile tests were conducted at room temperature with a mechanical tester (Instron ElectroPuls E10000) equipped with a 500 N load cell. For each PEG amount, three or more films (5 cm × 1.5 cm, length × width; 100–150 μm, thickness) were measured. The Young's modulus of each specimen was calculated by the linear fitting of stress–strain curves at low strain (<1%). DMA was performed at room temperature with a DMA 2980 (TA Instruments) in the thin-film testing configuration using the same sample size as for tensile tests. The tests were carried out in in frequency sweeping mode from 100 to 0.01 Hz. The oscillation amplitude was 30 μm. The static force applied to the sample was 0.01 N.

Swelling Test: PEDOT:PSS films were weighed by an analytic balance (Sartorius BP 210 D) right after baking to record their initial mass and successively soaked in DI water or transferred into a Cole-Parmer humidity-controlled chamber (03323-14) for 10–30 min. They were then removed from the water and transferred onto a piece of lint-free paper using tweezers. The water on the surface of the films was dried off and the samples were weighed for a second time. The mass increase of each sample was calculated using the following formula, where M_w is the mass of the wet film and M_D is mass of dry film.

$$\text{Weight Increase } (\%) = \frac{M_w - M_D}{M_D} \times 100 \qquad (1)$$

Films containing glycerol or PEG are easy to peel off from the glass substrate after baking and stable during water soaking process. Swelling of pristine PEDOT:PSS films could not be assessed, because they are difficult to handle and break apart when soaked in water.

Supporting Information

Supporting Information is available from the Wiley Online Library or from the author.

Conflict of Interest

The authors declare no conflict of interest.

[1] Y. J. Tan, J. Wu, H. Li, B. C. Tee, *ACS Appl. Mater. Interfaces* **2018**, *10*, 15331.

[2] M. W. Urban, D. Davydovich, Y. Yang, T. Demir, Y. Zhang, L. Casabianca, *Science* **2018**, *362*, 220.

[3] A. Campanella, D. Döhler, W. H. Binder, *Macromol. Rapid Commun.* **2018**, *39*, 1700739.

[4] P. Baek, N. Aydemir, Y. An, E. W. C. Chan, A. Sokolova, A. Nelson, J. P. Mata, D. McGillivray, D. Barker, J. Travas-Sejdic, *Chem. Mater.* **2017**, *29*, 8850.

[5] Y. Cao, Y. J. Tan, S. Li, W. W. Lee, H. Guo, Y. Cai, C. Wang, B. C.-K. Tee, *Nat. Electron.* **2019**, *2*, 75.

[6] J. Y. Oh, S. Kim, H. K. Baik, U. Jeong, *Adv. Mater.* **2016**, *28*, 4455.

[7] J. Kang, J. B. H. Tok, Z. Bao, *Nat. Electron.* **2019**, *2*, 144.

[8] S. Kee, M. A. Haque, D. Corzo, H. N. Alshareef, D. Baran, *Adv. Funct. Mater.* **2019**, *29*, 1905426.

[9] B. C. Tee, C. Wang, R. Allen, Z. Bao, *Nat. Nanotechnol.* **2012**, *7*, 825.

[10] C.-H. Li, C. Wang, C. Keplinger, J.-L. Zuo, L. Jin, Y. Sun, P. Zheng, Y. Cao, F. Lissel, C. Linder, *Nat. Chem.* **2016**, *8*, 618.

[11] Y. Liu, M. Pharr, G. A. Salvatore, *ACS Nano* **2017**, *11*, 9614.

[12] Z. Zou, C. Zhu, Y. Li, X. Lei, W. Zhang, J. Xiao, *Sci. Adv.* **2018**, *4*, eaaq0508.

[13] Q. Wu, J. Wei, B. Xu, X. Liu, H. Wang, W. Wang, Q. Wang, W. Liu, *Sci. Rep.* **2017**, *7*, 41566.

[14] S. Pati, B. P. Singh, S. Dhakate, in *Smart Polymer Nanocomposites* (Eds: D. Ponnamma, K. K. Sadasivuni, J.-J. Cabibihan, M. A.-A. Al-Maadeed), Springer, Berlin **2017**, p. 119.

[15] B. C. Tee, J. Ouyang, *Adv. Mater.* **2018**, *30*, 1802560.

[16] J. Kang, D. Son, O. Vardoulis, J. Mun, N. Matsuhisa, Y. Kim, J. Kim, J. B. H. Tok, Z. Bao, *Adv. Mater. Technol.* **2019**, *4*, 1800417.

[17] K. Parida, G. Thangavel, G. Cai, X. Zhou, S. Park, J. Xiong, P. S. Lee, *Nat. Commun.* **2019**, *10*, 2158.

[18] P. Song, H. Qin, H.-L. Gao, H.-P. Cong, S.-H. Yu, *Nat. Commun.* **2018**, *9*, 2786.

[19] Y. Cao, T. G. Morrissey, E. Acome, S. I. Allec, B. M. Wong, C. Keplinger, C. Wang, *Adv. Mater.* **2017**, *29*, 1605099.

[20] Y. Lu, Z. Liu, H. Yan, Q. Peng, R. Wang, M. E. Barkey, J.-W. Jeon, E. K. Wujcik, *ACS Appl. Mater. Interfaces* **2019**, *11*, 20453.

[21] B. J. Blaiszik, S. L. Kramer, M. E. Grady, D. A. McIlroy, J. S. Moore, N. R. Sottos, S. R. White, *Adv. Mater.* **2012**, *24*, 398.

[22] A. J. Bandodkar, V. Mohan, C. S. López, J. Ramírez, J. Wang, *Adv. Electron. Mater.* **2015**, *1*, 1500289.

[23] S. A. Odom, S. Chayanupatkul, B. J. Blaiszik, O. Zhao, A. C. Jackson, P. V. Braun, N. R. Sottos, S. R. White, J. S. Moore, *Adv. Mater.* **2012**, *24*, 2578.

[24] T. Wang, Y. Zhang, Q. Liu, W. Cheng, X. Wang, L. Pan, B. Xu, H. Xu, *Adv. Funct. Mater.* **2018**, *28*, 1705551.

[25] J. Dahlke, S. Zechel, M. D. Hager, U. S. Schubert, *Adv. Mater. Interfaces* **2018**, *5*, 1800051.

[26] R. Tamate, K. Hashimoto, T. Horii, M. Hirasawa, X. Li, M. Shibayama, M. Watanabe, *Adv. Mater.* **2018**, *30*, 1802792.

[27] X. Shi, X. Zhou, Y. Zhang, X. Xu, Z. Zhang, P. Liu, Y. Zuo, H. Peng, *J. Mater. Chem. C* **2018**, *6*, 12774.

[28] J. Xu, P. Chen, J. Wu, P. Hu, Y. Fu, W. Jiang, J. Fu, *Chem. Mater.* **2019**, *31*, 7951.

[29] E. J. Markvicka, M. D. Bartlett, X. Huang, C. Majidi, *Nat. Mater.* **2018**, *17*, 618.

[30] J. Chen, J. Liu, T. Thundat, H. Zeng, *ACS Appl. Mater. Interfaces* **2019**, *11*, 18720.

[31] J. Deng, X. Kuang, R. Liu, W. Ding, A. C. Wang, Y. C. Lai, K. Dong, Z. Wen, Y. Wang, L. Wang, *Adv. Mater.* **2018**, *30*, 1705918.

[32] K. Chu, B. G. Song, H. I. Yang, D. M. Kim, C. S. Lee, M. Park, C. M. Chung, *Adv. Funct. Mater.* **2018**, *28*, 1800110.

[33] Q. Wang, S. Ling, X. Liang, H. Wang, H. Lu, Y. Zhang, *Adv. Funct. Mater.* **2019**, *29*, 1808695.

[34] Y. Han, X. Wu, X. Zhang, C. Lu, *Adv. Mater. Technol.* **2019**, *4*, 1800424.

[35] K. Parida, J. Xiong, X. Zhou, P. S. Lee, *Nano Energy* **2019**, *59*, 237.

[36] S. Zhang, F. Cicoira, *Adv. Mater.* **2017**, *29*, 1703098.

[37] S. S. Katiyar, V. Kushwah, C. P. Dora, R. Y. Patil, S. Jain, *AAPS PharmSciTech* **2019**, *20*, 186.

[38] Y. Li, S. Zhang, X. Li, V. R. N. Unnava, F. Cicoira, *Flexible Printed Electron.* **2019**, *4*, 044004.

[39] D. A. Mengistie, P.-C. Wang, C.-W. Chu, *J. Mater. Chem. A* **2013**, *1*, 9907.

[40] L. Ouyang, C. Musumeci, M. J. Jafari, T. Ederth, O. Inganäs, *ACS Appl. Mater. Interfaces* **2015**, *7*, 19764.

[41] K.-m. Choi, M.-C. Choi, D.-H. Han, T.-S. Park, C.-S. Ha, *Eur. Polym. J.* **2013**, *49*, 2356.

[42] O. E. Geiculescu, B. B. Hallac, R. V. Rajagopal, S. E. Creager, D. D. DesMarteau, O. Borodin, G. D. Smith, *J. Phys. Chem. B* **2014**, *118*, 5135.

[43] Z. Zhu, G. Yang, R. Li, T. Pan, *Microsyst. Nanoeng.* **2017**, *3*, 17004.

[44] T. Ekblad, G. Bergström, T. Ederth, S. L. Conlan, R. Mutton, A. S. Clare, S. Wang, Y. Liu, Q. Zhao, F. D'Souza, *Biomacromolecules* **2008**, *9*, 2775.

[45] C. S. Gudipati, C. M. Greenlief, J. A. Johnson, P. Prayongpan, K. L. Wooley, *J. Polym. Sci., Part A: Polym. Chem.* **2004**, *42*, 6193.

[46] M. R. Moraes, A. C. Alves, F. Toptan, M. S. Martins, E. M. Vieira, A. J. Paleo, A. P. Souto, W. L. Santos, M. F. Esteves, A. Zille, *J. Mater. Chem. C* **2017**, *5*, 3807.

[47] X. Wang, G. Feng, M. Li, M. Ge, *Polym. Bull.* **2019**, *76*, 2097.

[48] H. S. Mansur, R. L. Oréfice, A. A. Mansur, *Polymer* **2004**, *45*, 7193.

[49] R. R. Mohamed, R. S. Seoudi, M. W. Sabaa, *Adv. Polym. Technol.* **2015**, *34*, 21479.

[50] M. Hayashi, F. Tournilhac, *Polym. Chem.* **2017**, *8*, 461.

[51] Q. Yin, Y. Peng, S. Zhang, F. Zhu, W. Li, K. Du, *Polym. Chem.* **2018**, *9*, 1164.

[52] J. Y. Oh, M. Shin, J. B. Lee, J.-H. Ahn, H. K. Baik, U. Jeong, *ACS Appl. Mater. Interfaces* **2014**, *6*, 6954.

[53] S.-S. Yoon, D.-Y. Khang, *J. Phys. Chem. C* **2016**, *120*, 29525.

[54] N. Kim, S. Kee, S. H. Lee, B. H. Lee, Y. H. Kahng, Y. R. Jo, B. J. Kim, K. Lee, *Adv. Mater.* **2014**, *26*, 2268.

[55] L. Bießmann, L. P. Kreuzer, T. Widmann, N. Hohn, J.-F. Moulin, P. Muller-Buschbaum, *ACS Appl. Mater. Interfaces* **2018**, *10*, 9865.

[56] B. Sarkar, M. Jaiswal, D. K. Satapathy, *J. Phys.: Condens. Matter* **2018**, *30*, 225101.

[57] M. ElMahmoudy, S. Inal, A. Charrier, I. Uguz, G. G. Malliaras, S. Sanaur, *Macromol. Mater. Eng.* **2017**, *302*, 1600497.

[58] P. Li, K. Sun, J. Ouyang, *ACS Appl. Mater. Interfaces* **2015**, *7*, 18415.